Proceedings of the ASME 2024 43rd International Conference on Ocean, Offshore and Arctic Engineering
OMAE2024
June 9-14, 2024, Singapore, Singapore

OMAE2024-127325

IMPACTS OF VESSEL MOTION ON THE DYNAMIC RESPONSE OF ROV SYSTEM IN THE PROCESSES OF DEPLOYMENT AND RECOVERY

Yucheng Guo[1,2], Xiaoqi Yu[1,2], Shuangxi Guo[1,2], Xiangxu Liu[1,2], Yue Kong[3], Weimin Chen[1,2]

[1]Institute of Mechanics, Chinese Academy of Sciences, Beijing, China
[2]School of Engineering Science, University of Chinese Academy of Sciences, Beijing, China
[3]School of Naval Architecture & Ocean Engineering, Jiangsu University of Science and Technology, Zhenjiang, China

ABSTRACT

Remotely operated vehicles (ROVs) are frequently used in subsea explorations and exploitations, aiming to obtain not only traditional ocean oil and gas, but also other mineral resources, such as manganese, polymetallic nodules and sulfides. However, due to the interactions between ocean environmental loads, ROV, suspending cable and top-end vessel, the dynamic responses of ROV system have strong coupling and nonlinear characteristics. Especially, during the initial deployment and the final recovery stages, the cable length might be so short that the relative motion between the ROV and the vessel may cause a severe collision and even structural damage. In this study, based on the structural and dynamic characteristics of the ROV system during the initial deployment and the final recovery stages, numerical simulation and analytical method are employed to investigate the impacts of the top-end vessel motion on the ROV system. In the numerical simulations, vessel surge and hydrodynamic force on ROV, are considered, and the ROV responses and cable tensions under different vessel motion amplitudes and frequencies are presented. It is found that the ROV responses are larger than the vessel motion amplitudes in some cases owing to vessel surge. And, the governing equation of ROV with a horizontal moving boundary is developed. Then, in order to have a deeper understand of the behaviors of the ROV system and the mechanisms of our simulation results, the analytical method is used.

Keywords: ROV system; deployment and recovery; dynamic response; vessel surge; numerical simulation

NOMENCLATURE

x_A	Vessel surge displacement [m]
x_0	Vessel surge amplitude [m]
ω	Vessel surge frequency [rad/s]
F	Hydrodynamic force [N]
C_D	Drag coefficient
C_m	Added mass coefficient
ρ	Density of seawater [kg/m^3]
v	ROV velocity [m/s]
M_0	Displaced water mass of ROV [kg]
η	Frequency ratio
α	Amplitude ratio
l	Cable length [m]
ω_0	Natural frequency of ROV system [rad/s]
G_{ROV}	ROV weight in water [N]
M	ROV mass in air [kg]
m	ROV added mass [kg]
T	Kinetic energy of system [N·m]
U	Potential energy of system [N·m]
θ	ROV angular displacement around the vessel [radian]
$x(t)$	ROV horizontal relative displacement [m]
x_{max}	Amplitude of ROV horizontal displacement [m]
Q	Response amplification factor
$\tilde{Q}$	Approximate response amplification factor
Q_s	Response amplification factor in the steady-state phase
ξ	Damping ratio

1. INTRODUCTION

Remotely operated vehicle (ROV) is a kind of submersible with deep-sea operation capability, which is widely used in the underwater survey, the oceanographic and geologic data acquisition [1, 2], the construction, inspection, maintenance, and repair of marine structures [3, 4], and the maritime search and rescue [5]. The ROV system is usually composed of top-end vessel, umbilical cable and underwater vehicle (ROV). The vessel provides power and transmits instructions to the ROV through the cable, and they transmit data to each other in real time [6, 7].

The main working steps of a ROV system include deployment, diving, operation, moving upward and recovery. In

order to ensure that the work is carried out in an orderly manner, it is particularly important to grasp the motion state of ROV and the reliability of cable or other structures in these processes. Therefore, the current researches related to ROV mainly concentrate on the two major fields of "ROV motion and positioning control" and "structural safety analysis". Among them, the structural safety analysis focuses on the motion and tension of the cable. However, due to the interactions between ocean environmental loads, ROV, cable and top-end vessel, the dynamic responses of ROV system have strong coupling and nonlinear characteristics. This makes the study of ROV system, during the whole operation processes, more challenging.

Accurate control is an important basis to ensure the autonomy and safety of ROV. The marine environment is complex, changeable and uncertain, making the control model uncertainty high. Therefore, the motion and positioning control technology of ROV has always been a difficult issue in the field of submersible research. However, most of these literatures focus on the operation stage of ROV [8-11], and rarely consider the two key stages of deployment and recovery. Especially, during the initial deployment and the final recovery stages, the ROV is in the wave zone and very close to the top-end vessel due to the shorter cable length. The vessel motion causes the ROV to oscillate, which has effect on the dynamic response of the ROV, and may even cause the collision between the ROV and the vessel due to the relative motion, resulting in the risk of damage. At the same time, the ROV motion will also change the cable tension, which causes the cable to slack or be shocked, seriously affecting the structural safety. Therefore, it is necessary to systematically analyze the ROV response and the cable tension during the deployment and recovery process.

Fewer literatures focusing on the ROV deployment and recovery processes are seen. Sayer [12] measured the wave forces on the scale model of a working-class ROV during deployment and recovery, and compared them with the results obtained from Morison's equation. Using numerical simulation, Tran et al. [13] studied the influence of the parameters of control system algorithms on the ROV tracking performance and umbilical tension during recovery process. Based on the experiments in the wave flume, Lubis et al. [14] studied the effects of vessel motion and winch speed on cable tension during a lightweight ROV passing through splash zone, and they put forward suggestions on the deployment and recovery strategy of ROV.

In this study, the dynamic responses of ROV system under the vessel surge are investigated, while the hydrodynamic force on ROV is included. The dynamic response of the ROV system is a complicated nonlinear problem, and it is difficult to directly obtain the accurate solution by an analytical method. Therefore, in this study, the FEM numerical simulations are used to examine the responses of the ROV system. Then, in order to have a deeper understand of the behaviors of the ROV system and the mechanisms of our simulation results, the analytical model, under the assumption of small response amplitude, is used. In Section 2, the finite element structural model and the hydrodynamic model of the ROV system are developed based on the structural and dynamic characteristics of the ROV system during the initial deployment and the final recovery stages. Section 3 shows the numerical simulation results of ROV displacement and cable tension under various cases, and the influences of vessel motion amplitude and frequency on the system response are examined. In Section 4, the ROV governing equation with a horizontal moving boundary is established and the laws presented in the numerical simulation results are further discussed. Section 5 is our research remarks.

2. ANALYSIS MODELS OF ROV SYSTEM

During the initial deployment and the final recovery stages, the vessel moves under the ocean environment loads, making the ROV oscillate around the vessel. In these processes, the bending and tensile deformations of the cable are much smaller than the rigid body motions of ROV, because the length of suspending cable is not large. Therefore, based on the structural and dynamic characteristics of the ROV system, we simplify the system as a pendulum with a moving boundary. The schematic diagram of the ROV system is shown in Fig.1. The boundary condition of the system is the motion of the top end of the cable, which is connected to the vessel. And it is assumed that the ROV is in still water, and the hydrodynamic force comes from the relative motion between the ROV and the fluid. The schematic diagram of the reference systems is shown in Fig.2. The fixed coordinate system on the surface of the still water serves as the inertial reference system S_1, and the moving vessel serves as the non-inertial reference system S_2. In this study, the motion of the vessel is assumed as a harmonic motion. In the reference system S_1, the vessel motion is described as:

$$x_A = x_0 \sin \omega t \tag{1}$$

where x_A is the vessel surge displacement, x_0 is the amplitude of the vessel surge motion, and ω is the frequency of the vessel surge motion.

In order to study the dynamic responses of ROV system caused by the vessel surge, a finite element model of the system composed of ROV and cable is established, and the effect of hydrodynamic force on ROV is also considered. The horizontal displacement excitation is applied to the first node of the cable to simulate the vessel surge motion. At the initial moment, the cable is vertically stationary and the ROV is in a stationary hovering state. The main parameters of ROV and cable are shown in Table 1, with reference to the parameters of the 4500m-class deep-sea operational ROV in Ref. [15].

2.1 Finite element structural model

The finite element simulation is used in this study to model the cable, and the whole cable is divided into a set of beam elements. The ROV is treated as a lumped mass suspended at the bottom end of the cable, or a lumped mass element is used to model the ROV. We assume that the motion of the ROV is in the $X-Y$ plane (see Fig.1), so only the plane displacements are

considered for each beam element. The displacement vector of the beam element is:

$$U_e = [u_i \quad v_i \quad \theta_i \quad u_{i+1} \quad v_{i+1} \quad \theta_{i+1}]^T \tag{2}$$

where u and v are the axial and translational displacements, respectively. θ is the rotational angle, and i is the node number of the beam element. For simplicity, the displacement vector is divided into two parts, i.e., the axial part and the lateral part:

$$\begin{aligned} U_e^1 &= [u_i \quad u_{i+1}]^T \\ U_e^2 &= [v_i \quad \theta_i \quad v_{i+1} \quad \theta_{i+1}]^T \end{aligned} \tag{3}$$

The shape function matrices of beam element are:

$$\begin{aligned} N_1(x_e) &= \left[1 - \frac{x_e}{l_e}, \frac{x_e}{l_e}\right] \\ N_2(x_e) &= [1 - 3\xi^2 + 2\xi^3, l_e(\xi - 2\xi^2 + \xi^3), 3\xi^2 \\ &\quad -2\xi^3, l_e(\xi^3 - \xi^2)] \end{aligned} \tag{4}$$

where l_e is the length of the element, which is 0.2m in the numerical model. x_e is the axial location and $\xi = x_e/l_e$.

The strain matrix can be written as:

$$B_i(x_e) = \frac{d(N_i)}{d(x_e)} \tag{5}$$

Then the mass and stiffness matrices of the element can be written as:

$$\begin{aligned} K_e^1 &= \int_0^{l_e} \int_{A_e} B_1^T E_e B_1 \, dA_e dx_e \\ M_e^1 &= \int_0^{l_e} \int_{A_e} B_1^T \rho A_e B_1 \, dA_e dx_e \\ K_e^2 &= \int_0^{l_e} \int_{A_e} B_2^T E_e B_2 \, dA_e dx_e \\ M_e^2 &= \int_0^{l_e} \int_{A_e} B_2^T \rho A_e B_2 \, dA_e dx_e \end{aligned} \tag{6}$$

where ρ is the density of the cable, A_e is the cross area, and E_e is the Young's modulus of the cable. The first two equations are used to describe the mass and stiffness matrices in the axial direction, and the latter two are about the lateral direction.

For the cable that only provides tension and no compression stiffness, the cable response is simulated by an improved finite element model. In our improved finite element model, the rotation DOFs of beam elements are not constrained. Then the rotational DOF θ will change into θ, θ', and Eq. (2) describing the displacement vector of each element is rewritten as:

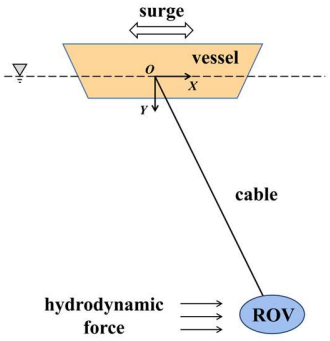

FIGURE 1: ILLUSTRATION OF ROV SYSTEM.

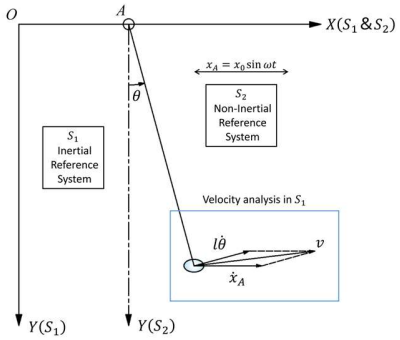

FIGURE 2: SCHEMATIC OF THE REFERENCE SYSTEMS.

TABLE 1: MAIN PARAMETERS OF ROV AND ITS CABLE

Parameter	Value
ROV body sizes (m)	3.1×1.8×2.0
ROV mass in air (kg)	4187.5
Displaced water mass of ROV (kg)	3350
Cable length (m)	10
Cable external diameter (m)	0.04
Cable mass in water (kg/m)	1.26×10^{-2}
Cable Young's modulus (GPa)	200

$$\begin{aligned} \boldsymbol{U}_i' &= [u_i \; v_i \; \theta_i \; \theta_i' \; u_{i+1} \; v_{i+1} \; \theta_{i+1} \; \theta_{i+1}']^T \\ i &= 2, \cdots, N-1 \end{aligned} \tag{7}$$

It is seen that, because of the additional DOF θ', the stiffness matrix has singularity. To eliminate this singularity, we use additional constrains, i.e., an original shape calculated through traditional static method. For the cable structures with different tensile and compressive stiffness, the response of the cable at different stages is simulated by customizing the stress-strain relationship of the material. Assembling the element matrices, the whole structural matrices are obtained, and then the dynamic governing equation, in terms of finite element expression, of the cable is:

$$[M] \cdot [\ddot{U}] + [C] \cdot [\dot{U}] + [K] \cdot [U] = [P] \quad (8)$$

where $[M]$, $[C]$ and $[K]$ are the mass matrix, damping matrix and stiffness matrix, respectively. $[U]$ and $[P]$ are the displacement vector and load vector of the whole cable, respectively. The damping matrix is calculated by Rayleigh damping commonly used in engineering. The calculation expression of the damping matrix is as follows:

$$[C] = \alpha_1[M] + \alpha_2[K] \quad (9)$$

where α_1 and α_2 are the proportional coefficients.

To solve the Eq. (8), the Newmark scheme is used to integrate in time. Assuming the current time step is step n, an estimate of the acceleration at the end of step $n+1$ will satisfy the following equation of motion:

$$[M] \cdot [a_{n+1}] + [C] \cdot [v_{n+1}] + [K] \cdot [d_{n+1}] = [p_{n+1}] \quad (10)$$

where $[p_{n+1}]$, $[a_{n+1}]$, $[v_{n+1}]$ and $[d_{n+1}]$ are the vectors of externally applied loads, estimated acceleration, estimated velocity and estimated displacement at step $n+1$, respectively. The estimates of displacement and velocity are given by:

$$[d_{n+1}] = [d_n] + [v_n]\Delta t + \frac{(1-2\beta)[a_n]\Delta t^2}{2}\beta[a_{n+1}]\Delta t^2$$
$$[v_{n+1}] = [v_n] + (1-\gamma)[a_n]\Delta t + \gamma[a_{n+1}]\Delta t \quad (11)$$

where Δt is the time step, β and γ are constants, and the values of β and γ are 1/6 and 1/2 respectively in this study.

2.2 Hydrodynamic model

In this study, we use Morison's equation to calculate the hydrodynamic force on the ROV, which is a sum of an initial force proportional to acceleration and a drag force proportional to the square of velocity. And the drag force on the ROV can be regarded as the nonlinear damping effect. The hydrodynamic force on the ROV in still water can be written as [15,16]:

$$\boldsymbol{F} = -\frac{1}{2}C_D\rho L^2\boldsymbol{v}|\boldsymbol{v}| - C_m M_0\dot{\boldsymbol{v}} \quad (12)$$

where ρ is the density of seawater, and it is $1025kg/m^3$; L is the characteristic length, and it is taken as the ROV width of $1.8m$; v is the ROV velocity; M_0 is the displaced water mass of ROV; C_D is the drag coefficient, and C_m is the added mass coefficient. ROVs have complex external structures and there are large differences between the structures of different ROVs, making it difficult to generalize the hydrodynamic performances of ROVs. Compared to CFD simulation and empirical formula, the model test is a better way to obtain hydrodynamic coefficients of ROV. Here, C_D is taken as 0.28 [15], and C_m is taken as 0.8 [14].

The established FEM model and method, including the cable structural model and the moving boundary, along with the combination of hydrodynamic force during dynamic response, have been verified in our previous publications [17,18]. Considering the length of the paper, the verification process and examples of the model are not given in the paper.

3. NUMERICAL SIMULATION RESULTS

The dynamic responses of the ROV system, including the ROV responses and the cable tensions, caused by the surge motion of the vessel are obtained based on the numerical simulations. For the convenience of discussion, two parameters describing the vessel motion are defined: the amplitude ratio α and the frequency ratio η. The amplitude ratio is the ratio of the vessel motion amplitude x_0 to the cable length l, and the frequency ratio is the ratio of the vessel motion frequency ω to the natural frequency of the ROV system ω_0. In this study, we fixed the cable length to 10 m, and the natural frequency of the ROV system is 0.3457 rad/s (0.0550 Hz). The simulated cases are shown in Table 2. In this section, by comparing the ROV responses and cable tensions under different cases, the impacts of parameters on the dynamic responses of the ROV system are summarized.

TABLE 2: SIMULATED CASES.

Amplitude ratio α	Frequency ratio η
0.05	0.5, 0.7, 0.9, 1.0, 1.1, 1.5, 2.0, 3.0
0.075	0.5, 0.7, 1.0, 1.1, 1.5, 3.0
0.1	0.5, 0.7, 0.9, 1.0, 1.1, 1.5, 2.0, 3.0
0.125	0.5, 0.7, 1.0, 1.1, 1.5, 3.0
0.15	0.5, 0.7, 1.0, 1.1, 1.5, 3.0
0.2	0.5, 0.7, 1.0, 1.1, 1.5, 3.0

3.1 ROV response

The horizontal displacement relative to the vessel is used here to indicate the ROV response. Fig.3 illustrates the ROV displacement histories at different frequency ratios, with two amplitude ratios of 0.05 and 0.1 at each frequency ratio. It can be seen that the frequency of ROV response increases as the excitation frequency increases. When the frequency ratios are in the non-resonance region, it is observed from Figs.2(a)-(b) and (f)-(h) that in the transient-state phase, the ROV displacement increases rapidly to the peak amplitude, and then decays to the steady-state amplitude. And when the frequency ratios are in the resonance region, it is observed from Figs.2(c)-(e) that the peak value of the response amplitude increases significantly, but the amplitude grows at a slower rate. Specifically, when the frequency ratio is equal to 1.0, the maximum amplitude in the transient-state phase is the steady-state amplitude, while when the frequency ratio is not equal to 1.0, the maximum amplitude in the transient-state phase is slightly larger than the steady-state amplitude.

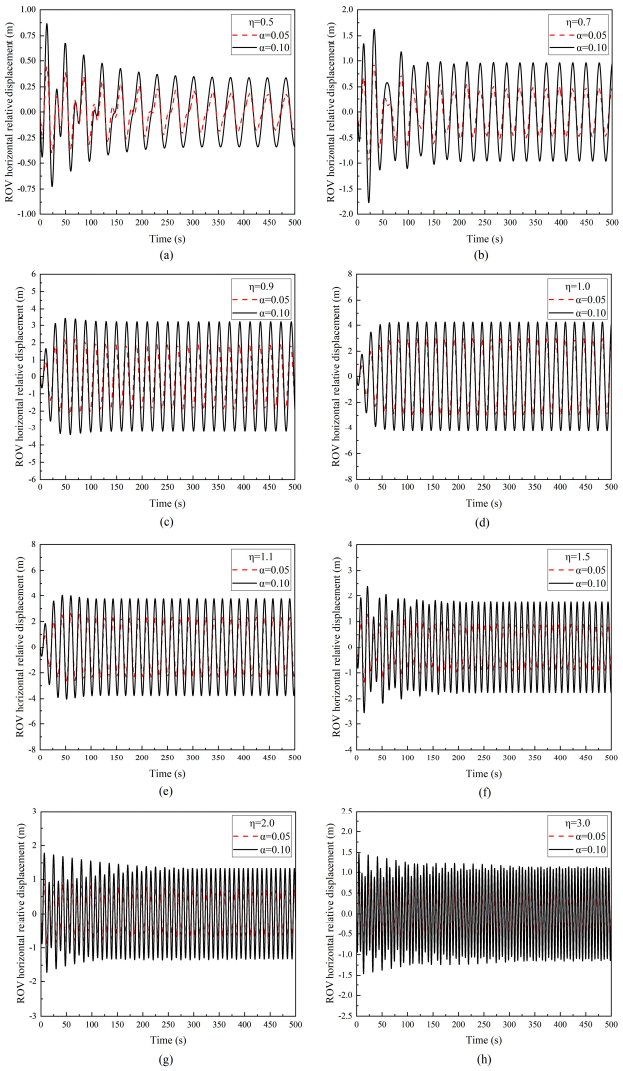

FIGURE 3: THE ROV DISPLACEMENT HISTORIES UNDER DIFFERENT FREQUENCY RATIOS: (a) $\eta = 0.5$, (b) $\eta = 0.7$, (c) $\eta = 0.9$, (d) $\eta = 1.0$, (e) $\eta = 1.1$, (f) $\eta = 1.5$, (g) $\eta = 2.0$, (h) $\eta = 3.0$.

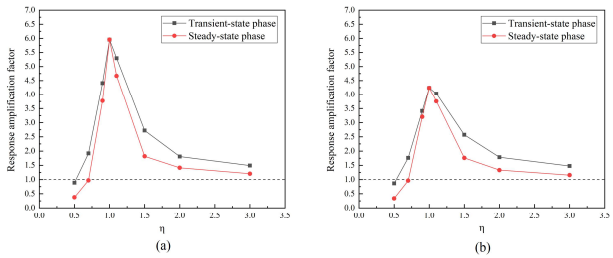

FIGURE 4: THE CHANGE OF RESPONSE AMPLIFICATION FACTOR OF THE ROV DISPLACEMENT WITH FREQUENCY RATIO IN THE TRANSIENT-STATE AND STEADY-STATE PHASES: (a) AT $\alpha = 0.05$, (b) AT $\alpha = 0.1$.

The ratio of the maximum value of the response amplitude to the amplitude of the vessel motion is defined as the response amplification factor. Fig.4 illustrates the change of response amplification factor of the ROV displacement with frequency ratio. The change trends of the response amplification factor are similar at the amplitude ratios of 0.05 and 0.1. The response amplification factors increase first and then decrease with the frequency ratio, and reach the peaks when the frequency ratio is equal to 1.0, e.g. when the amplitude ratio is 0.05, the response amplification factor reaches 5.955. The peak values of the ROV response in the transient-state phase are larger than those in the steady-state phase (except for the resonance case). And the difference of which have maximums near the frequency ratios of 0.7 and 1.5. In addition, when the frequency ratio is larger than 0.7, the response amplification factor is always larger than 1, that is, the ROV response is amplified compared to the amplitude of vessel motion owing to vessel surge. It indicates that the frequency ratio of 0.7 is a critical case.

Fig.5 illustrates the changes of response amplitude and response amplification factor of the ROV displacement with amplitude ratio. When the frequency ratio is in the non-resonance region, the ROV response amplitude increases linearly with the amplitude ratio, while the response amplification factors are nearly constant, which indicates that the frequency ratio is the main parameter to control the amplification effect of the vessel surge on the ROV response. When the frequency ratio is in the resonance region, the ROV response amplitude shows a weak nonlinear growth trend, while the ROV response amplification factor gradually decreases with the amplitude ratio. It is because as the frequency ratio approaches 1, the system response is stronger as the amplitude ratio increases, making the stiffness nonlinear effect larger and the damping effect more significant.

3.2 Structural tension of suspending cable

Fig.6 shows the numerical simulation results of cable tension amplification factor (the ratio of the maximum value of the cable tension to the ROV weight in water) under different frequency ratios and amplitude ratios. It can be observed that the cable tension amplification factor is always larger than 1.

By observing the trend of the curves in Fig.6(a), it is found that the change of the tension amplification factor with frequency ratio is non-monotonic in both transient-state and the steady-state phases. The peak value of the cable tension reaches a local maximum near the frequency ratio of 1 (up to 1.20 times the ROV weight at the amplitude ratio of 0.1), and between the frequency ratio of 1.5 and 2, there exists a local minimum. The cable tension mainly depends on the inertial centrifugal force generated by the ROV oscillating around the vessel, which is proportional to the square of the ROV velocity. And the amplitude of ROV velocity is related to the response amplification factor. Based on the response amplification factor in the resonance region considering damping in Section 4.3.2, there exists a maximum of the ROV velocity near $\eta = 1$. When $\eta > 1.5$, the damping effect is weak, according to the response amplification factor in the steady-state phase without

considering damping in Section 4.2, there exists a minimum of the ROV velocity at $\eta = \sqrt{3}$. Therefore, the results of analytical method and numerical simulation are consistent.

As shown in Fig.6 (b), it can be seen that the tension amplification factor shows a weak nonlinear characteristic with the change of amplitude ratio. The amplitude of ROV velocity varies linearly with α, so the tension amplification factor varies linearly with α^2. In addition, the change gradient of the tension amplification factor increases with the increase of frequency ratio.

4. DISCUSSIONS

4.1 Governing equation of ROV with a horizontal moving boundary

In the reference system S_1 (see Fig.2), the ROV velocity $\boldsymbol{v}$ is expressed as Eq. (13). And the fluid particles and the ROV are regarded as a system. The total kinetic energy of the system is the kinetic energy of the ROV considering the added mass, and the total potential energy of the system is the sum of the potential energy of the fluid particle and the ROV. Taking the origin of the coordinate as the zero potential energy point, the expressions of kinetic energy T and potential energy U of the system are obtained:

$$\boldsymbol{v} = \dot{\boldsymbol{x}}_{\boldsymbol{A}} + \dot{\boldsymbol{\theta}} \times \boldsymbol{l} \tag{13}$$

$$T = \frac{1}{2}(M+m)\left(\dot{x}_A{}^2 + \dot{\theta}^2 l^2\right) - (M+m)\dot{\theta} l \cos\theta \, \dot{x}_A \tag{14}$$

$$U = U_w - (M - M_0) g l \cos\theta \tag{15}$$

where $\dot{x}_A$ is the velocity of vessel motion, θ is the ROV angular displacement around the vessel in the reference system S_2, $\dot{\theta}$ is the angular velocity, M is the ROV mass in air, m is the ROV added mass, M_0 is the displaced water mass of ROV, g is the gravitational acceleration, and U_w is the potential energy of the fluid particles distributed in the whole space domain, which is a constant.

Based on the numerical simulation results in Section 3, it can be deduced that the damping effect on ROV response induced by the hydrodynamic force is small, so the damping is not considered firstly. Let $\omega_0 t = \tau$, ${\omega_0}^2 = \frac{g}{l} \cdot \frac{M - M_0}{M + m}$, and the Lagrangian function be $L = T - U$, which are substituted into the Lagrange equation. Ignoring the infinitesimal of higher order, the governing equation for the ROV motion with a horizontal moving boundary is developed:

$$\ddot{\theta} + \theta = -\alpha\eta^2 \sin\eta\tau \tag{16}$$

4.2 ROV response amplification factor without damping

Under the small response amplitude, it is approximated that the ROV horizontal relative displacement $x(t)$ obtained from

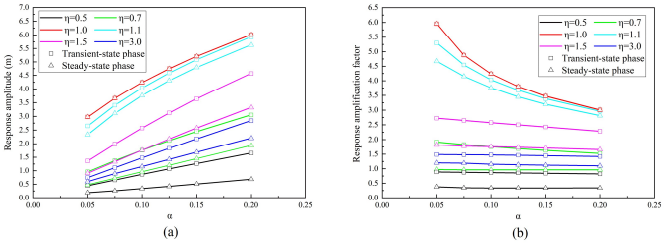

FIGURE 5: THE RESULTS OF THE ROV RESPONSE IN THE TRANSIENT-STATE AND STEADY-STATE PHASES UNDER DIFFERENT AMPLITUDE RATIOS: (a) RESPONSE AMPLITUDE, (b) RESPONSE AMPLIFICATION FACTOR.

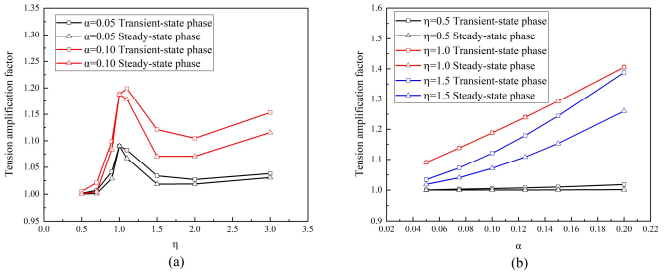

FIGURE 6: THE CHANGES OF CABLE TENSION AMPLIFICATION FACTOR WITH FREQUENCY RATIO AND AMPLITUDE RATIO: (a) FREQUENCY RATIO, (b) AMPLITUDE RATIO.

the numerical simulation is the product of the ROV angular displacement θ and the cable length l. Therefore, the characteristics of horizontal relative displacement and angular displacement of ROV are similar. Eq. (16) is a typical governing equation for forced vibration. When the ROV is at rest at the initial moment, i.e., $\theta = 0$ and $\dot{\theta} = 0$, the solution of the governing equation is shown in Eq. (17):

$$\theta(t) = \frac{x(t)}{l} = -\frac{\alpha\eta^2}{1-\eta^2}(\sin\eta\tau - \eta\sin\tau) \tag{17}$$

It can be seen that the amplitude ratio only affects the response amplitude, while the frequency ratio not only affects the amplitude of the ROV response but also change pattern. The first term in Eq. (17) is the steady-state response, and the second term is the transient-state response. By analyzing the extreme values of this equation, the exact expression of the response amplification factor without damping is obtained:

$$Q = \frac{x_{max}}{x_0} = max\left\{\frac{\eta^2}{1+\eta}\sin\left(\frac{2k\pi}{1-\eta}\right), \frac{\eta^2}{1-\eta}\sin\left(\frac{2k\pi}{1+\eta}\right)\right\} \tag{18}$$

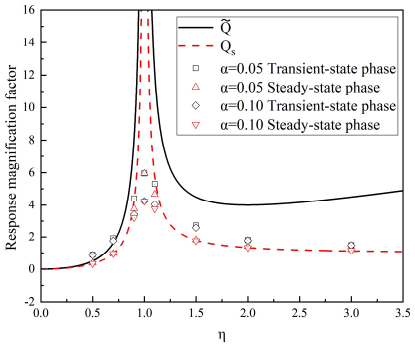

FIGURE 7: THE CHANGES OF $\tilde{Q}$, Q_s AND RESPONSE AMPLIFICATION FACTOR OBTAINED BY NUMERICAL SIMULATION WITH FREQUENCY RATIO.

where x_{max} is the amplitude of ROV horizontal relative displacement, and k is any positive integer. Since the above equation is complicated, it is approximated as $\tilde{Q} = \frac{\eta^2}{1-\eta}$. Because the sine function is approximated as 1, this approximate response amplification factor $\tilde{Q}$ is larger than the exact one.

When damping exists, the transient-state response gradually attenuates with time, and when only the steady-state response remains, the system is in the steady-state phase. And the response amplification factor in the steady-state phase Q_s is shown in Eq. (19). Fig.7 demonstrates the changes of $\tilde{Q}$ and Q_s with frequency ratio. It can be seen that $\tilde{Q}$ is significantly larger than Q_s when the frequency ratio is relatively large, because the transient-state response is amplified with the increase of frequency ratio.

$$Q_s = \frac{\eta^2}{1-\eta^2} \tag{19}$$

4.3 Analysis of the numerical simulation results

The ROV responses without damping are discussed both in Section 4.1 and Section 4.2. The numerical simulation results are analyzed below considering the effect of hydrodynamic damping.

4.3.1 The ROV response in the resonance region

Assuming that the damping ratio ξ is very small, the ROV response is expressed as:

$$\begin{aligned} x(t) &= \frac{\alpha l \eta^2}{\sqrt{(1-\eta^2)^2+4\eta^2\xi^2}}\sin(\omega t+\phi) \\ &\quad + \frac{\alpha l \eta^3 e^{-\xi\omega_0 t}}{\sqrt{(1-\eta^2)^2+4\eta^2\xi^2}}\cos(\omega_0 t+\psi) \\ \tan\phi &= -2\frac{\eta}{1-\eta^2}\xi, \quad \tan\psi = \frac{1-\eta^2}{2\xi} \end{aligned} \tag{20}$$

Based on the above equation, when the frequency ratio, the cable length and the damping ratio are determined, the response amplitude is proportional to the amplitude ratio in both transient-state and steady-state phases. It is consistent with the phenomenon that the response amplitude increases linearly with amplitude ratio as shown in Fig.5(a).

When the excitation frequency is in the resonance region, it is mentioned in Section 3.1 that the ROV response grows slowly to the peak amplitude in the transient-state phase. At this time, the amplitude and frequency between the transient-state and steady-state responses are not much different. And the effect of damping on the response is significant. In order to obtain the expression of ROV response in the resonance region, substituting $\omega = \omega_0 + \varepsilon$ (ε is a small quantity) into the Eq. (20):

$$\begin{aligned} x(t) &= \frac{\alpha l \eta^2}{\sqrt{(1-\eta^2)^2+4\eta^2\xi^2}}\Phi(t)\sin\omega t \\ \Phi^2(t) &\approx 1+\eta^2 e^{-2\xi\omega_0 t} \\ &\quad -2e^{-\xi\omega_0 t}[\eta\cos\varepsilon t - \xi\sin\varepsilon t] \end{aligned} \tag{21}$$

In order to clarify the change of the response amplitude with time, we let $\tau = \omega_0 t$ and derive the time-varying function $\Phi^2(t)$ in the response amplitude of Eq. (21):

$$\begin{aligned} \frac{d}{dt}\Phi^2 \approx 2\omega_0 e^{-\xi\tau}\cdot[&(2\eta-1)\xi\cos(\eta-1)\tau \\ &-(\xi^2-\eta^2+\eta)\sin(\eta-1)\tau - \xi\eta^2 e^{-\xi\tau}] \end{aligned} \tag{22}$$

It can be seen that when $\eta = 1$, Eq. (22) becomes $\frac{d}{dt}\Phi^2 = 2\xi\omega_0 e^{-\xi\tau}(1-e^{-\xi\tau})$, which is always larger than zero, indicating that the response amplitude increases monotonically from zero to steady-state amplitude. When $\eta \neq 1$, the derivative function $\frac{d}{dt}\Phi^2$ has the infinite number of zero points, so the process of the response reaching the steady-state phase is observed to be oscillatory in Figs.2(c) and (e), but the oscillation amplitude is extremely small.

4.3.2 Influences of vessel motion frequency on ROV response amplification factor

In Section 4.2, the relationship between the amplification factor of ROV response and the frequency ratio without damping is obtained, and the theoretical results are compared with the numerical simulation results in the following. The symbols in Fig.7 are the response amplification factors obtained by numerical simulation at amplitude ratios of 0.05 and 0.1, respectively. It can be seen that in the non-resonance region ($|\eta - 1| > 0.15$), the numerical simulation results in the steady-state phase fit well with Eq. (19). This suggests that if the excitation frequency is within the non-resonance region, the undamped linear theory can well predict the ROV response in the steady-state phase. Meanwhile, by observing Eq. (19), the

number of the solution of equation $Q_s = 1$ is only one, i.e., $\eta = \sqrt{2}/2 \approx 0.7$. And it can be further proved that the response amplification factor in the steady-state phase is always larger than one when the frequency ratio is larger than 0.7, which also corresponds to the results presented in Fig.4. However, when the excitation frequency is in the resonance region ($|\eta - 1| < 0.15$), the response is very sensitive to damping, and even a small damping will produce a large suppression effect. So that the response peaks in both the steady-state and transient-state phases are much smaller than the theoretical results. In order to grasp the ROV response in the resonance region more accurately, the damping is introduced into the expression of response amplification factor, as shown in Eq. (23):

$$Q = \frac{\eta^2}{\sqrt{(1-\eta^2)^2+4\eta^2\xi^2}} \tag{23}$$

4.3.3 Influences of vessel motion amplitude on ROV response

The change gradients of the response amplitude related to the amplitude ratio in the steady-state and transient-state phases are:

$$g_s = \frac{\eta^2 l}{\sqrt{(1-\eta^2)^2+4\eta^2\xi^2}} \tag{24}$$

$$g_t = \frac{\eta^2 l}{\sqrt{(1-\eta^2)^2+4\eta^2\xi^2}}\left[1 + \eta e^{-\xi\omega_0 t_1}\right] \tag{25}$$

where t_1 is the moment corresponding to the peak value of response in the transient-state phase. t_1 is larger as the frequency ratio approaches to 1. The change gradients increase as the frequency ratio approaches 1, indicating that the system is closer to resonance, the ROV response amplitude is more sensitive to the change of the amplitude ratio, which is consistent with the phenomenon observed in Fig.5 (a).

5. CONCLUSIONS

In this study, through FEM numerical simulation, the dynamic responses of ROV system, including ROV responses and cable tensions, under the vessel surge and hydrodynamic force, are obtained. The influences of important parameters, such as amplitude ratio and frequency ratio, which characterize the vessel motion conditions, on the system responses are summarized. At the same time, their physical essences are explained by theoretical analysis.

The vessel motion amplitude only affects the amplitude of the ROV response, not the change pattern. The amplitude of the ROV response increases approximately linearly with the vessel motion amplitude. While, as the vessel motion frequency approaches to the natural frequency of the ROV system, the growth gradient is larger and shows a nonlinear trend. Meanwhile, the cable tension increases nonlinearly with the vessel motion amplitude, and the growth gradient increases as the vessel motion frequency increases.

The vessel motion frequency not only affects the amplitude of the ROV response but also the change pattern: (a) As the vessel motion frequency approaches to the natural frequency of the ROV system, the ROV response amplitude is larger. At this time, the hydrodynamic damping has a significant effect on the ROV response, and the damping increases with the increase of the vessel motion amplitude, suppressing the amplification effect of the vessel motion on the ROV response. In contrast, when the vessel motion frequency is not in the resonance region, the damping has no obvious effect on the ROV response, and this nonlinear phenomenon will not occur. (b) Except for the case of the frequency ratio of 1, the ROV response amplitude in the transient-state phase is larger than that in the steady-state phase, and the amplitude attenuation from the transient-state phase to the steady-state phase varies non-monotonically with the frequency ratio. (c) When the frequency ratio is larger than 0.7, the amplitude of ROV response is larger than that of the vessel surge motion. As for the cable tension, the change of the response peak value with the frequency ratio is also non-monotonic. When the frequency ratio is less than 2, there exists a maximum of the tension amplitude near $\eta = 1$, which can reach 1.20 times the ROV weight. While when the frequency ratio is larger than 2, the cable tension amplitude increases monotonically with frequency ratio.

REFERENCES

[1] Q. Li, Y. Cao, B. Li, D. M. Ingram, A. Kiprakis, Numerical Modelling and Experimental Testing of the Hydrodynamic Characteristics for an Open-Frame Remotely Operated Vehicle, Journal of Marine Science and Engineering 8(9) (2020) 688.

[2] S. Soylu, A. A. Proctor, R. P. Podhorodeski, C. Bradley, B. J. Buckham, Precise trajectory control for an inspection class ROV, Ocean Engineering 111 (2016) 508-523.

[3] O. A. N. Eidsvik, I. Schjølberg, Finite element cable-model for Remotely Operated Vehicles (ROVs) by application of beam theory, Ocean Engineering 163 (2018) 322-336.

[4] R. Gabl, et al., Hydrodynamic loads on a restrained ROV under waves and current, Ocean Engineering 234 (2021) 109279.

[5] W. Quan, Y. Liu, A. Zhang, X. Zhao, X. Li, The nonlinear finite element modeling and performance analysis of the passive heave compensation system for the deep-sea tethered ROVs, Ocean Engineering 127 (2016) 246-257.

[6] D. Khojasteh, R. Kamali, Design and dynamic study of a ROV with application to oil and gas industries of Persian Gulf, Ocean Engineering 136 (2017) 18-30.

[7] D. D. A. Fernandes, A. J. Sørensen, K. Y. Pettersen, D. C. Donha, Output feedback motion control system for observation class ROVs based on a high-gain state observer: Theoretical and experimental results, Control Engineering Practice 39 (2015) 90-102.

[8] L. G. García-Valdovinos, T. Salgado-Jiménez, M. Bandala-Sánchez, L. Nava-Balanzar, R. Hernández-Alvarado, J. A. Cruz-Ledesma, Modelling, Design and Robust Control of a

Remotely Operated Underwater Vehicle, International Journal of Advanced Robotic Systems 11(1) (2014) 1.

[9] R. Hernández-Alvarado, L. García-Valdovinos, T. Salgado-Jiménez, A. Gómez-Espinosa, F. Fonseca-Navarro, Neural Network-Based Self-Tuning PID Control for Underwater Vehicles, Sensors 16(9) (2016) 1429.

[10] Z. Chu, D. Zhu, S. X. Yang, Observer-Based Adaptive Neural Network Trajectory Tracking Control for Remotely Operated Vehicle, IEEE Trans. Neural Netw. Learning Syst. 28(7) (2017) 1633–1645.

[11] S. Jin, J. Kim, J. Kim, T. Seo, Six-Degree-of-Freedom Hovering Control of an Underwater Robotic Platform With Four Tilting Thrusters via Selective Switching Control, IEEE/ASME Trans. Mechatron. 20(5) (2015) 2370–2378.

[12] P. Sayer, Hydrodynamic loads during the deployment of ROVs, Ocean Engineering 35.1 (2008) 41-46.

[13] C. Tran, et al., Operability analysis of control system for ROV launch-and-recovery from autonomous surface vessel, Ocean Engineering 277 (2023) 114272.

[14] M. B. Lubis, M. Kimiaei, Wave flume and numerical test on launch and recovery of ultra-deep-water ROV through splash zone under wave and ship motion, Ocean Engineering 238 (2021) 109767.

[15] S. Fan, Hydrodynamics Test and Research on Motion Control for Deep Sea Work-Class Remotely Operated Vehicle, Doctoral dissertation, Shanghai: Shanghai Jiao Tong University, 2013.

[16] Det Norske Veritas, Environmental conditions and environmental loads, DNVGL-RP-C205, 2019.

[17] Y. Li, S. Guo, W. Chen, et al., Analysis on restoring stiffness and its hysteresis behavior of slender catenary mooring-line, Ocean Engineering 209 (2020) 107521.

[18] Y. Li, S. Guo, Y. Guo, et al., Dynamic responses and robustness performance to moving boundary of double-stepped cable during deep-sea mining, International Journal of Naval Architecture and Ocean Engineering 15 (2023) 100546.